Application of the Boundary-Element Method to Waveguide Discontinuities

MASANORI KOSHIBA, SENIOR MEMBER, IEEE, AND
MICHIO SUZUKI, SENIOR MEMBER, IEEE

Abstract — **A numerical method for the solution of scattering of the *H*- and *E*-plane waveguide junctions is described. The approach is a combination of the boundary-element method and the analytical method. A general computer program has been developed using the quadratic elements (higher order boundary elements). To show the validity and usefulness of this formulation, computed results are given for a right-angle corner bend, a T-junction, an inductive strip-planar circuit mounted in a waveguide, a waveguide-type dielectric filter, and an inhomogeneous waveguide junction, and a linear taper. Comparison of the present results with the results of the finite-element method shows good agreement.**

I. Introduction

Waveguide discontinuities play an important role in designing microwave circuits [1], [2], and theoretical and experimental studies of waveguide discontinuity scattering problems have occupied the attention of numerous researchers for several decades. Recently, a numerical approach based on the finite-element method (FEM) has been developed for the analysis of planar circuits [3], [4], and *H*- and *E*-plane waveguide junctions [5]–[7]. The FEM is very useful for the arbitrarily shaped discontinuities. However, it requires a large computer memory and long computation time to solve the final matrix equation. More recently, the boundary-element method (BEM) [8], [9] has been applied to the *H*-plane junctions [10]–[12] and the planar circuits [13]. The BEM is one of the 'boundary'-type methods based on the integral equation method which has already been successfully applied to open-boundary planar circuits in 1972 [14] and to short-boundary planar circuits in 1975 [15], [16]. It is therefore possible to reduce the matrix dimension and to use computer memory more economically compared with the 'domain'-type method, such as the FEM. However, in [10], [11], [14], and [15], it is assumed that the waveguide propagates a single mode only and the evanescent modes are neglected. Therefore, it seems to be difficult to obtain accurate results over a wide range of frequencies. Furthermore, in [10]–[16], the constant elements [8], [9] or the linear elements [8], [9] are used to divide the boundary of the two-dimensional region. Generally, it is difficult to reduce the energy error with these boundary elements. In [12], the linear elements are used and the condition of power conservation is satisfied to an accuracy of about ± 4 percent. In order to obtain more accurate results, fairly many elements are necessary, and, thus, the merits of the BEM are lost. In the FEM analysis using the quadratic triangular elements (higher order finite elements), on the other hand, the energy error is less than 0.1 percent [5]–[7].

In this paper, the combined method of the BEM with the quadratic line elements (higher order boundary elements) and the analytical method is described for the analysis of scattering by the *H*- or *E*-plane waveguide junctions. To show the validity and usefulness of this formulation, computed results are given for various *H*- and *E*-plane waveguide discontinuities. Comparison of the results of the BEM with those of the FEM [5]–[7] shows good agreement. In the present BEM analysis, the power condition is satisfied to an accuracy of $\pm 10^{-4}$ to 10^{-3}.

II. Basic Equations

In order to minimize the detail, we consider the waveguide junction as shown in Fig. 1, where the boundary Γ_i connects the discontinuities to the rectangular waveguide i ($i=1, 2$), d_i is the width a_i or the height b_i of the waveguide i for the *H*- or *E*-plane junction, respectively; the region Ω surrounded by Γ_1, Γ_2, and the short-circuit boundary Γ_0 completely encloses the waveguide discontinuities, and the waveguide i is assumed to be filled with dielectric of relative permittivity ϵ_{ri}.

Considering the excitation by the dominant TE_{10} mode, we have the following basic equation:

$$\frac{\partial^2 \phi}{\partial x^2} + \frac{\partial^2 \phi}{\partial y^2} + \hat{k}^2 \phi = 0 \tag{1}$$

$$\hat{k}^2 = k_0^2 \hat{\epsilon}_r \tag{2}$$

$$k_0^2 = \omega^2 \epsilon_0 \mu_0 \tag{3}$$

$$\phi = \begin{cases} E_z, & \text{for } H\text{-plane junction} \\ H_z, & \text{for } E\text{-plane junction} \end{cases} \tag{4}$$

$$\hat{\epsilon}_r = \begin{cases} \epsilon_r, & \text{for } H\text{-plane junction} \\ \epsilon_r - (\pi/k_0 a)^2, & \text{for } E\text{-plane junction} \end{cases} \tag{5}$$

where ω is the angular frequency, E_z and H_z are the electric and

Manuscript received May 14, 1985; September 27, 1985.
The authors are with the Department of Electronic Engineering, Hokkaido University, Sapporo, 060, Japan.
IEEE Log Number 8406478.

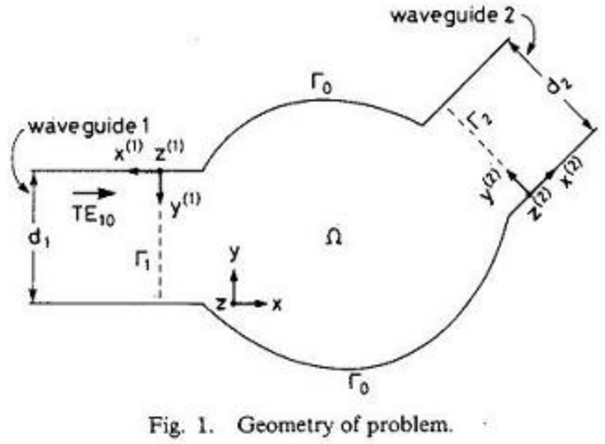

Fig. 1. Geometry of problem.

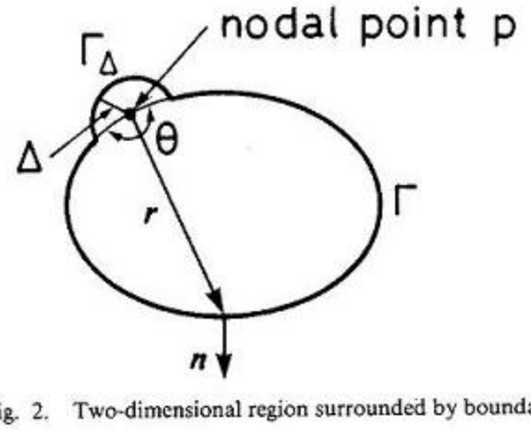

Fig. 2. Two-dimensional region surrounded by boundary Γ.

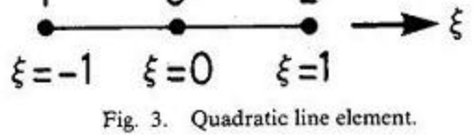

Fig. 3. Quadratic line element.

magnetic fields, respectively, and ϵ_0 and μ_0 are the permittivity and permeability of free space, respectively.

III. Mathematical Formulation

A. Boundary-Element Approach[1]

Considering the region surrounded by the boundary Γ as shown in Fig. 2, and using the fundamental solution ϕ^* [8], [9] and Green's formula, from (1) we obtain the following equation [10]–[13]:

$$\phi_p + \int_\Gamma \psi^* \phi \, d\Gamma = \int_\Gamma \phi^* \psi \, d\Gamma \tag{6}$$

where

$$\phi^* = \frac{1}{4j} H_0^{(2)}(\hat{k}r) \tag{7}$$

$$\psi^* = \frac{j}{4} \hat{k} H_1^{(2)}(\hat{k}r) \cos\alpha. \tag{8}$$

Here ϕ_p is the value of ϕ at the nodal point p, ψ, and ψ^* are the outward normal derivatives of ϕ and ϕ^*, respectively, $H_0^{(2)}$ and $H_1^{(2)}$ are the zeroth- and first-order Hankel functions of the second kind, respectively, and α is the angle between the vector $\boldsymbol{r}$ and the outward unit normal vector $\boldsymbol{n}$.

Noting that the nodal point p is placed on the boundary Γ and considering the integration path Γ_Δ going around the nodal point p as shown in Fig. 2, we obtain for (6)

$$\frac{\theta}{2\pi}\phi_p + \int\!\!\!\!\!\!-_\Gamma \psi^* \phi \, d\Gamma = \int\!\!\!\!\!\!-_\Gamma \phi^* \psi \, d\Gamma \tag{9}$$

where $\int\!\!\!\!\!\!-$ denotes the Cauchy's principal value of integration, namely $\int\!\!\!\!\!\!-_\Gamma = \lim_{\Delta \to 0} \int_{\Gamma - \Gamma_\Delta}$. Dividing the boundary Γ into quadratic line elements as shown in Fig. 3, ϕ and ψ within each element are defined in terms of ϕ_q and ψ_q at the nodal points q ($q = 1, 2, 3$), respectively, as follows:

$$\phi = \{N\}^T \{\phi\}_e \tag{10}$$

$$\psi = \{N\}^T \{\psi\}_e \tag{11}$$

where

$$\{\phi\}_e = [\phi_1 \phi_2 \phi_3]^T \tag{12}$$

$$\{\psi\}_e = [\psi_1 \psi_2 \psi_3]^T \tag{13}$$

$$\{N\} = [N_1 N_2 N_3]^T. \tag{14}$$

[1]Since a general formulation of the BEM with linear elements for analyzing two-dimensional electromagnetic fields is given in [11], only the outline of the BEM with quadratic elements will be described here.

Here T, $\{\cdot\}$, and $\{\cdot\}^T$ denote a transpose, a column vector, and a row vector, respectively, and the shape function N_q is given by

$$N_q = A_q \xi^2 + B_q \xi + C_q \tag{15}$$

$$A_1 = 1/2, \quad A_2 = 1/2, \quad A_3 = -1 \tag{16a}$$

$$B_1 = -1/2, \quad B_2 = 1/2, \quad B_3 = 0 \tag{16b}$$

$$C_1 = 0, \quad C_2 = 0, \quad C_3 = 1 \tag{16c}$$

with the normalized coordinate ξ defined on the eth element.

Substituting (10) and (11) into (9), we obtain

$$\frac{\theta}{2\pi}\phi_p + \sum_e \{h\}_e^T \{\phi\}_e = \sum_e \{g\}_e^T \{\psi\}_e \tag{17}$$

where

$$\{h\}_e = [h_1 h_2 h_3]^T \tag{18}$$

$$\{g\}_e = [g_1 g_2 g_3]^T. \tag{19}$$

Here Σ_e extends over all different elements. When the nodal point p does not belong to the eth element, h_q and g_q are calculated with Gaussian integration as

$$h_q = \frac{L}{2} \int_{-1}^{1} N_q \frac{j}{4} \hat{k} H_1^{(2)}(\hat{k}r) \cos\alpha \, d\xi \tag{20}$$

$$g_q = \frac{L}{2} \int_{-1}^{1} N_q \frac{1}{4j} H_0^{(2)}(\hat{k}r) \, d\xi \tag{21}$$

where L is the length of the element. When the nodal point p belongs to the eth element, calculations of h_q and g_q involve the limitation of $\Delta \to 0$. In this case, $\cos\alpha = 0$, so that

$$h_q = 0. \tag{22}$$

For the case where the nodal point p coincides with the nodal point $q = 1$, 2, or 3 of the eth element in Fig. 2, g_q is given by

$$g_q = (L/2)\left[A_q I_2(2) - (2A_q - B_q)\{I_1(2) - 2/(\pi \hat{k}^2 L^2)\} + (A_q - B_q + C_q) I_0(2)\right] \tag{23a}$$

$$g_q = (L/2)\left[A_q I_2(2) - (2A_q + B_q)\{I_1(2) - 2/(\pi \hat{k}^2 L^2)\} + (A_q + B_q + C_q) I_0(2)\right] \tag{23b}$$

or

$$g_q = L\left[A_q I_2(1) + C_q I_0(1)\right] \tag{23c}$$

respectively. Here I_0, I_1, and I_2 are calculated as follows:

$$I_0(\eta) = \int \frac{1}{4j} H_0^{(2)}\left(\frac{\hat{k}L}{2}\eta\right) d\eta$$
$$= -\frac{\eta}{4} \sum_{v=0}^{\infty} \frac{(-1)^v}{(2v+1)(v!)^2} \left(\frac{\hat{k}L}{4}\eta\right)^{2v}$$
$$\cdot \left[\frac{2}{\pi}\left(\gamma + \ln\left(\frac{\hat{k}L}{4}\eta\right)\right.\right.$$
$$\left.\left. - \frac{1}{2v+1} - \sum_{s=1}^{v} \frac{1}{s}\right) + j\right] \quad (24a)$$

$$I_1(\eta) = \int \frac{\eta}{4j} H_0^{(2)}\left(\frac{\hat{k}L}{2}\eta\right) d\eta$$
$$= \frac{1}{4j} \frac{2\eta}{\hat{k}L} H_1^{(2)}\left(\frac{\hat{k}L}{2}\eta\right) \quad (24b)$$

$$I_2(\eta) = \int \frac{\eta^2}{4j} H_0^{(2)}\left(\frac{\hat{k}L}{2}\eta\right) d\eta$$
$$= \left(\frac{2}{\hat{k}L}\right)^2 \left[\frac{\hat{k}L}{2} \frac{\eta^2}{4j} H_1^{(2)}\left(\frac{\hat{k}L}{2}\eta\right)\right.$$
$$\left. + \frac{\eta}{4j} H_0^{(2)}\left(\frac{\hat{k}L}{2}\eta\right) - I_0(\eta)\right] \quad (24c)$$

where γ is the Euler's number.

In the matrix notation, (17) is rewritten as follows [8]–[13]:

$$[H]\{\phi\} = [G]\{\psi\}. \quad (25)$$

From (25), the following equation is obtained for the waveguide junction in Fig. 1:

$$[[H]_0 \quad [H]_1 \quad [H]_2] \begin{bmatrix} \{\phi\}_0 \\ \{\phi\}_1 \\ \{\phi\}_2 \end{bmatrix}$$
$$= [[G]_0 \quad [G]_1 \quad [G]_2] \begin{bmatrix} \{\psi\}_0 \\ \{\psi\}_1 \\ \{\psi\}_2 \end{bmatrix} \quad (26)$$

where the subscripts 0, 1, and 2 denote the quantities corresponding to the boundaries Γ_0, Γ_1, and Γ_2 in Fig. 1, respectively.

B. Analytical Approach

Assuming that the dominant TE_{10} mode of unit amplitude is incident from the waveguide j ($j=1, 2$) in Fig. 1, ϕ on Γ_i ($i=1, 2$) may be expressed analytically as

$$\phi(x^{(i)}=0, y^{(i)}) = 2\delta_{ij} f_{j1}(y^{(j)})$$
$$- \sum_m \frac{1}{j\beta_{im}} \int_0^{d_i} f_{im}(y_0^{(i)}) f_{im}(y_0^{(i)})$$
$$\cdot \psi(x^{(i)}=0, y^{(i)})\, dy_0^{(i)} \quad (27)$$

where

$$f_{im}(y^{(i)}) = \sqrt{2/a_i} \sin m\pi y^{(i)}/a_i, \qquad m=1, 2, 3, \cdots \quad (28)$$

$$\beta_{im} = \sqrt{k_0^2 \epsilon_{ri} - (m\pi/a_i)^2}, \qquad m=1, 2, 3, \cdots \quad (29)$$

for the H-plane junction

$$f_{im}(y^{(i)}) = \sqrt{\sigma_n/b_i} \cos n\pi y^{(i)}/b_i, \qquad n=0, 1, 2, \cdots \quad (30)$$

$$\beta_{im} = \sqrt{k_0^2 \epsilon_{ri} - (\pi/a)^2 - (n\pi/b_i)^2}, \qquad n=0, 1, 2, \cdots \quad (31)$$

$$\sigma_n = \begin{cases} 1, & n=0 \\ 2, & n \neq 0 \end{cases} \quad (32)$$

for the E-plane junction, and δ_{ij} is the Kronecker δ.

Using (10) and (11), (27) can be discretized as follows:

$$\{\phi\}_i = \delta_{ij}\{f\}_j + [Z]_i\{\psi\}_i \quad (33)$$

where

$$\{f\}_j = 2\{f_1\}_j \quad (34)$$

$$[Z]_i = -\sum_m (1/j\beta_{im})\{f_m\}_i \sum_{\dot{e}} \int_{\dot{e}} f_{im}(y_0^{(i)})$$
$$\cdot \left\{N(x^{(i)}=0, y_0^{(i)})\right\} dy_0^{(i)}. \quad (35)$$

Here the components of the $\{f_m\}_i$ vector are the values of $f_{im}(y^{(i)})$ at the nodal points on Γ_i and $\Sigma_{\dot{e}}$ extends over the elements related to Γ_i.

C. Combination of Boundary-Element and Analytical Relations

Using (33), from (26) we obtain the following final matrix equation:

$$\left[\begin{array}{cccccc} [H]_0 & [H]_1 & [H]_2 & -[G]_0 & -[G]_1 & -[G]_2 \\ \hline [0] & [1] & [0] & [0] & -[Z]_1 & [0] \\ [0] & [0] & [1] & [0] & [0] & -[Z]_2 \end{array}\right]$$
$$\cdot \begin{bmatrix} \{\phi\}_0 \\ \{\phi\}_1 \\ \{\phi\}_2 \\ \{\psi\}_0 \\ \{\psi\}_1 \\ \{\psi\}_2 \end{bmatrix} = \left[\begin{array}{c} \{0\} \\ \{0\} \\ \{0\} \\ \{0\} \\ \hline \delta_{1j}\{f\}_j \\ \delta_{2j}\{f\}_j \end{array}\right] \quad (36)$$

where [1] is a unit matrix, [0] is a null matrix, and $\{0\}$ is a null vector. In (36), $\{\phi\}_0 = \{0\}$ and $\{\psi\}_0 = \{0\}$ should be considered for the H- and E-plane junctions, respectively.

The values of ϕ at nodal points on Γ_i, namely $\{\phi\}_i$, are computed from (36), and then $\phi(x^{(i)}=0, y^{(i)})$ on Γ_i can be calculated from (10). The solutions on Γ_i allow the determination of the scattering parameters S_{ij} of the TE_{10} mode as follows:

$$S_{jj} = \int_0^{d_j} \phi(x^{(j)}=0, y^{(j)}) f_{j1}(y^{(j)})\, dy^{(j)} - 1 \quad (37)$$

$$S_{ij} = \sqrt{\beta_{i1}\hat{\epsilon}_{rj}/\beta_{j1}\hat{\epsilon}_{ri}}$$
$$\cdot \int_0^{d_i} \phi(x^{(i)}=0, y^{(i)}) f_{i1}(y^{(i)})\, dy^{(i)}, \qquad i \neq j. \quad (38)$$

In (38), for the H-Plane junction, both $\hat{\epsilon}_{ri}$ and $\hat{\epsilon}_{rj}$ should be replaced by 1.

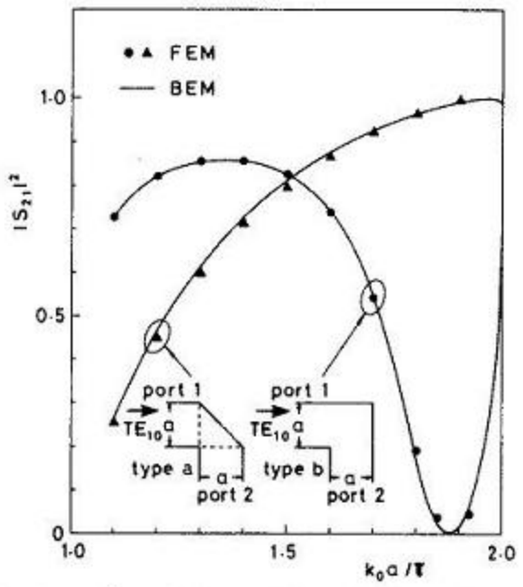

Fig. 4. Power transmission coefficient of right-angle corner bend.

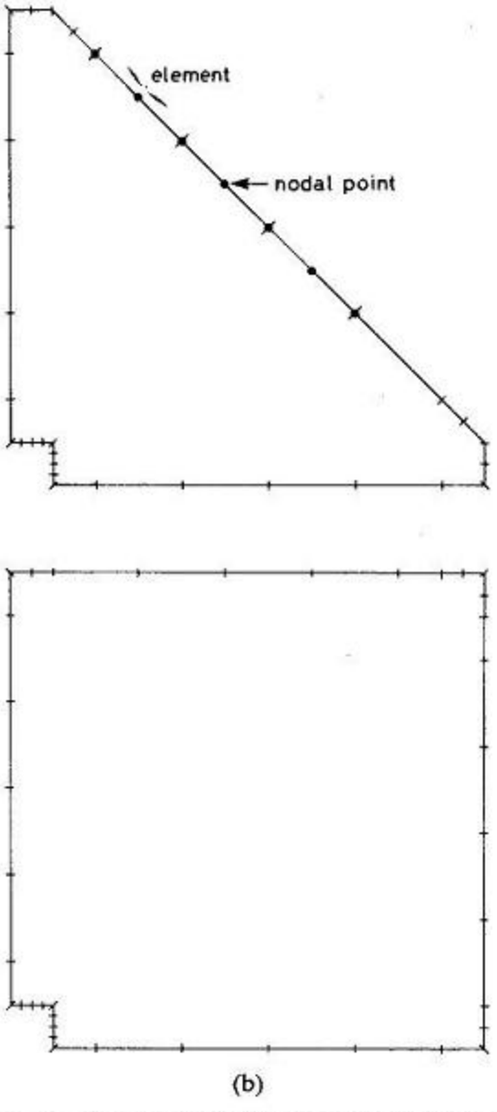

Fig. 5. Element division for right-angle corner bend.

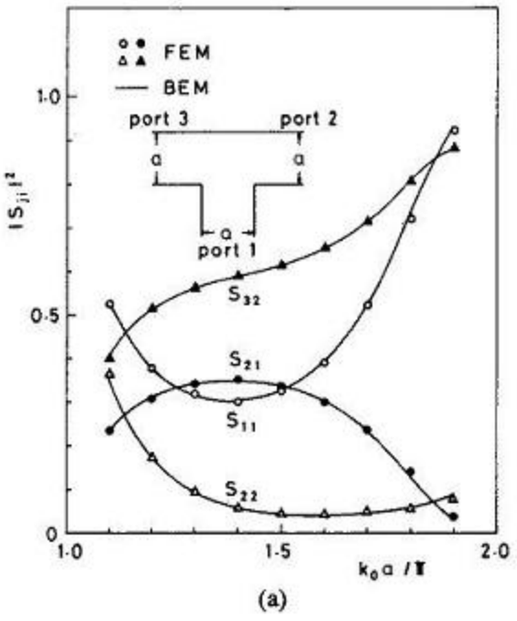

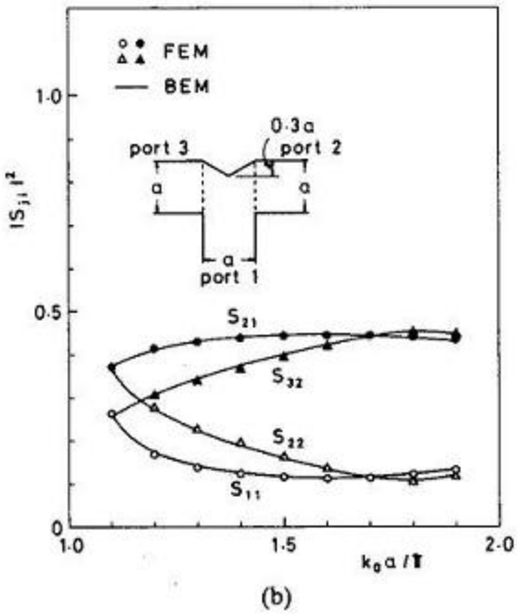

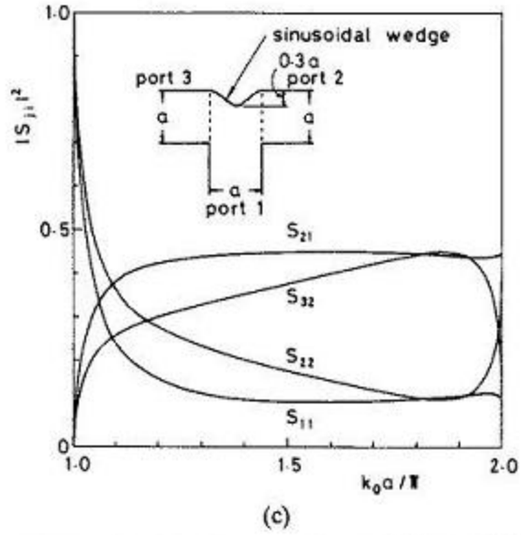

Fig. 6. Power reflection and transmission coefficients of T-junction.

IV. Computed Results

In this section, we present the computed results for various H- and E-plane waveguide discontinuities. Convergence of the solution is checked by increasing m in (35) and the number of the elements. Although the convergence is obtained by using the first three or four evanescent higher modes, in this analysis, the first six evanescent higher modes are used in (35). The results of the BEM agree well with those of the FEM [5]–[7] and agree well with the other theoretical results [15]–[20] and the experimental results [18], [19], [21]. For the H-plane waveguide discontinuities, the experimental results [18], [19] and the results of the integral equation method [15], [16], the normal-mode method [17]–[19], and the moment method [20] are not shown in this paper (these results are cited in [5] and [6]).

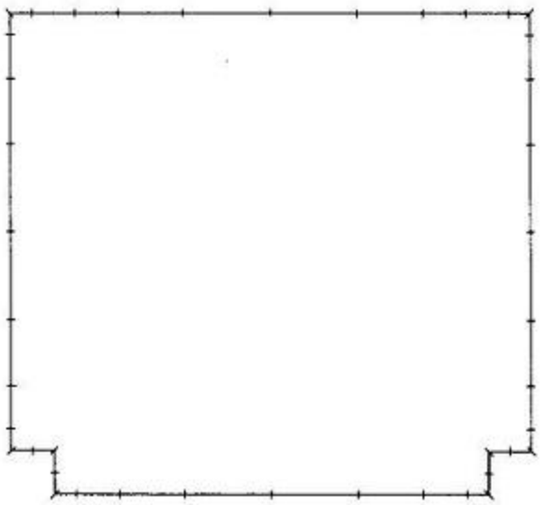

(a)

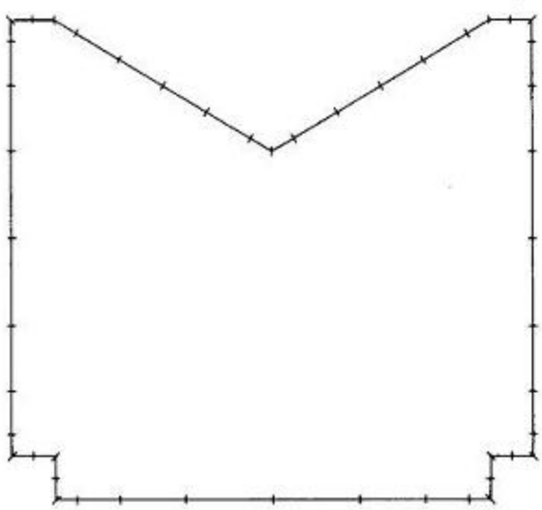

(b)

Fig. 7. Element division for T-junction.

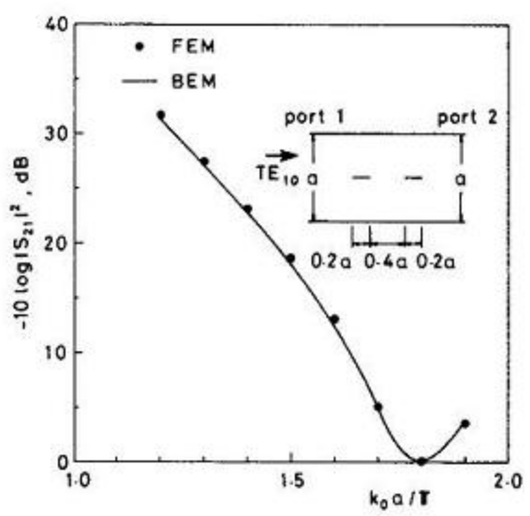

Fig. 8. Power transmission coefficient of inductive strip-planar circuit mounted in a waveguide.

A. H-Plane Junction

Fig. 4 shows the power transmission coefficient ($|S_{21}|^2$) of a right-angle corner bend. Fig. 5(a) and (b) shows the element divisions for the type *a* and the type *b* in Fig. 4, respectively.

The present approach can be applied easily to the analysis of multi-port junctions. Fig. 6 shows the power reflection coefficients ($|S_{11}|^2$ and $|S_{22}|^2$) and the power transmission coefficients ($|S_{21}|^2$ and $|S_{32}|^2$) of a T-junction. Fig. 7(a) and (b) shows the element divisions for the T-junction in Fig. 6(a) and the T-junction with wedge in Fig. 6(b), respectively. From Fig. 6(a)–(c), it is found that over a wide range of frequencies, the reflection at port 1 is reduced with a linear wedge (Fig. 6(b)) and that this reflection at port 1 may be further reduced with a sinusoidal wedge (Fig. 6(c)).

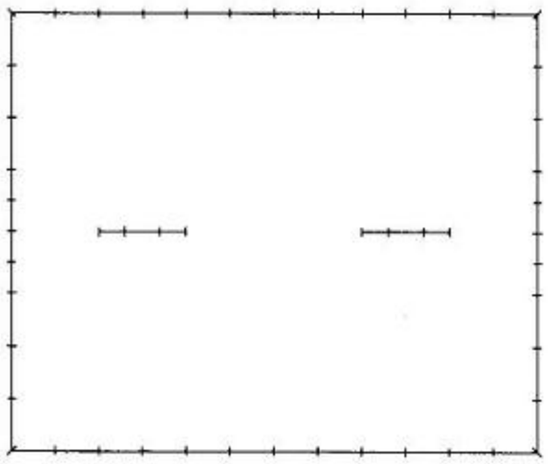

Fig. 9. Element division for inductive strip-planar circuit mounted in a waveguide.

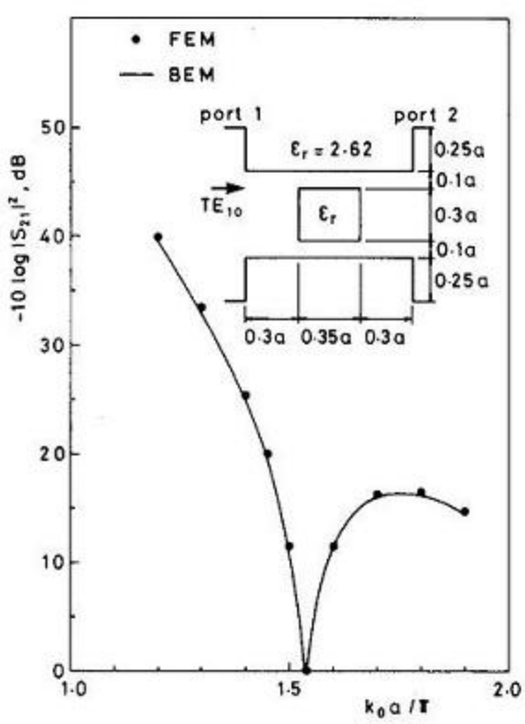

Fig. 10. Power transmission coefficient of waveguide-type dielectric filter.

Fig. 8 shows the power transmission coefficient of an inductive strip-planar circuit mounted in a waveguide. Fig. 9 shows the element division for this circuit. In this case, the boundary condition $\phi = 0$ should be considered on strip conductors.

The present approach can also be applied to the analysis of multi-media problems. A procedure of programming for handling multi-media problems is given in [11]. Fig. 10 shows the power transmission coefficient of a waveguide-type dielectric filter. Fig. 11 shows the element division for this filter. In this case, the boundary conditions $\phi_{air} = \phi_{dielectric}$ and $\psi_{air} = -\psi_{dielectric}$ should be considered on the interface between air and dielectric.

The present approach is applicable to the frequency range in which waveguide propagates multi-modes. Fig. 12(a) and (b) shows the magnitudes of reflection and transmission coefficients of an inhomogeneous waveguide junction, respectively. Fig. 13 shows the element division for this junction. For both reflection and transmission coefficients, the results of the BEM agree well with those of the FEM [6]. The results of the moment method [20] for the transmission coefficient are different from those of

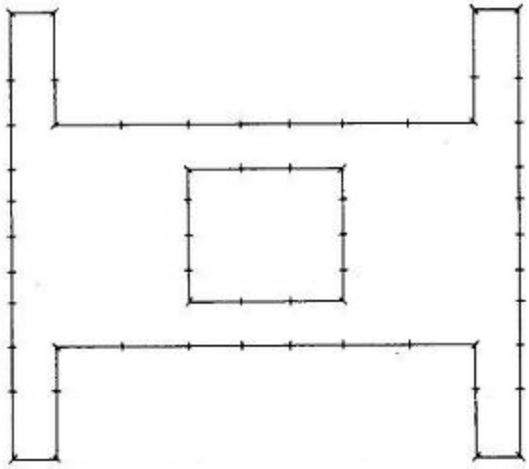

Fig. 11. Element division for waveguide-type dielectric filter.

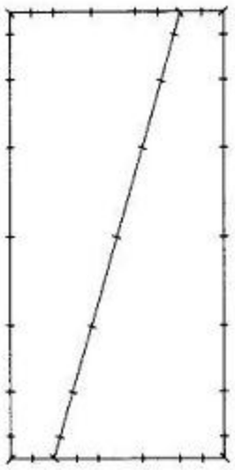

Fig. 13. Element division for inhomogeneous waveguide junction.

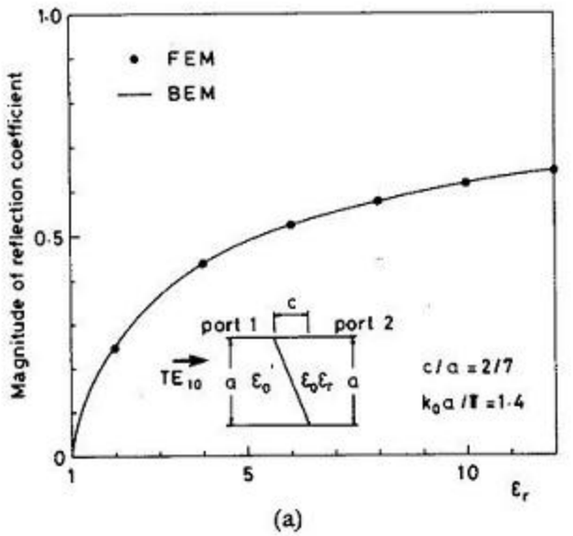

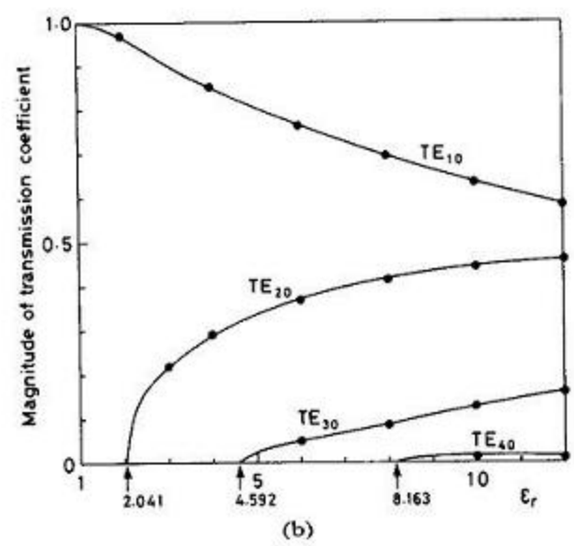

Fig. 12. Magnitudes of reflection and transmission coefficients of inhomogeneous waveguide junction.

TABLE I
NUMBER OF NODAL POINTS USED IN THE BEM AND FEM ANALYSES

H-plane junction	BEM	FEM
Fig.4 (type a)	62	299
Fig.4 (type b)	76	377
Fig.6 (a)	84	385
Fig.6 (b)	96	399
Fig.8	102	609
Fig.10	120	379
Fig.12	79	589

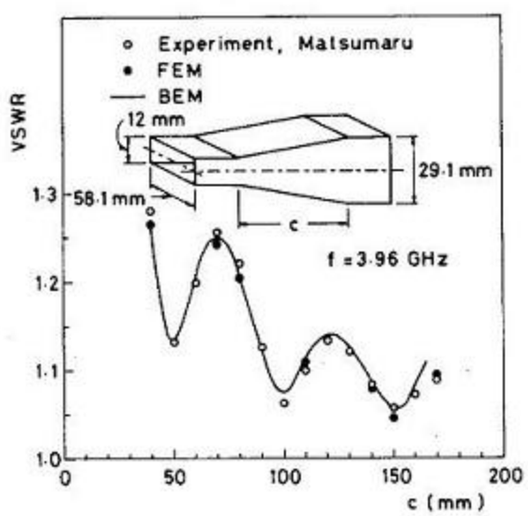

Fig. 14. VSWR characteristics of linear E-plane taper.

the BEM and the FEM. In the moment method, the transmission coefficients of the higher order modes are not zero at the cutoff values of ϵ_r.

Table I shows the number of the nodal points used in the BEM and FEM analyses of H-plane junctions. Here, in both BEM and FEM analyses, the symmetry of a circuit to reduce the dimensions of the matrices is not used. The accuracies of the present boundary-element calculations are almost identical to those of the earlier finite-element calculations [5], [6], and yet the BEM allows the matrix dimension to be reduced by a factor of about 7 to 3.

B. E-Plane Junction

A comparison of the results obtained applying the BEM to the linear E-plane tapers of various lengths with the experimental results [21] and the results of the FEM [7] is given in Fig. 14 and very good agreement is obtained.

V. CONCLUSION

A method of analysis, based on the boundary-element approach and the analytical approach, was developed for the solution of the H- and E-plane junctions. The validity of the method

was confirmed by comparing numerical results for various *H*- and *E*-plane waveguide discontinuities with the results of the finite-element method.

This approach can be applied easily to the planar circuits [3], [4], [13]. The problem of how to deal with waveguide junctions with lossy media or anisotropic media hereafter still remains.

Acknowledgment

The authors wish to thank T. Miki for his assistance in numerical computations.

References

[1] N. Marcuvitz, *Waveguide Handbook*. New York: McGraw-Hill, 1951.
[2] R. E. Collin, *Field Theory of Guided Waves*. New York: McGraw-Hill, 1960.
[3] P. Silvester, "Finite element analysis of planar microwave networks," *IEEE Trans. Microwave Theory Tech.*, vol. MTT-21, pp. 104–108, Feb. 1973.
[4] T. Miyoshi, "The expansion of electromagnetic field in planar circuit," *Trans. Inst. Electron. Commun. Eng. Japan*, vol. J58-B, pp. 84–91, Feb. 1975 (in Japanese).
[5] M. Koshiba, M. Sato, and M. Suzuki, "Application of finite-element method to *H*-plane waveguide discontinuities," *Electron. Lett.*, vol. 18, pp. 364–365, Apr. 1982.
[6] M. Koshiba, M. Sato, and M. Suzuki, "Finite-element analysis of arbitrarily shaped *H*-plane waveguide discontinuities," *Trans. Inst. Electron. Commun. Eng. Japan*, vol. E66, pp. 82–87, Feb. 1983.
[7] M. Koshiba, M. Sato, and M. Suzuki, "Application of finite-element method to *E*-plane waveguide discontinuities," *Trans. Inst. Electron. Commun. Eng. Japan*, vol. E66, pp. 457–458, July 1983.
[8] C. A. Brebbia, *The Boundary Element Method for Engineers*. London: Pentech Press, 1978.
[9] C. A. Brebbia and S. Walker, *Boundary Element Techniques in Engineering*. London: Butterworth, 1980.
[10] S. Washisu and I. Fukai, "An analysis of electromagnetic unbounded field problems by boundary element method," *Trans. Inst. Electron. Commun. Eng. Japan*, vol. J64-B, pp. 1359–1365, Dec. 1981 (in Japanese).
[11] S. Kagami and I. Fukai, "Application of boundary-element method to electromagnetic field problems," *IEEE Trans. Microwave Theory Tech.*, vol. MTT-32, pp. 455–461, Apr. 1984.
[12] K. Kanao and S. Kurazono, "Waveguide-type dielectric filter," *Trans. Inst. Electron. Commun. Eng. Japan*, vol. J67-B, pp. 1177–1178, Oct. 1984 (in Japanese).
[13] E. Tonye and H. Baudrand, "Multimode *S*-parameters of planar multiport junctions by boundary element method," *Electron. Lett.*, vol. 20, pp. 799–802, Sept. 1984.
[14] T. Okoshi and T. Miyoshi, "The planar circuit—An approach to microwave integrated circuitry," *IEEE Trans. Microwave Theory Tech.*, vol. MTT-20, pp. 245–252, Apr. 1972.
[15] T. Okoshi and S. Kitazawa, "Computer analysis of short-boundary planar circuit," *IEEE Trans. Microwave Theory Tech.*, vol. MTT-23, pp. 299–306, Mar. 1975.
[16] T. Okoshi and S. Kitazawa, "Computer analysis of short-boundary planar circuit," *Tech. Res. Rep. Inst. Electron. Commun. Eng. Japan*, MW75-75, Oct. 1975 (in Japanese).
[17] T. Anada and J. P. Hsu, "Analysis of planar circuit with short circuit boundary by normal mode method through impedance matrix," *Trans. Inst. Electron. Commun. Eng. Japan*, vol. J61-B, pp. 646–653, July 1978 (in Japanese).
[18] T. Anada, M. Hatayama, and J. P. Hsu, "Wide-band frequency characteristics of rectangular waveguide *H*-plane T-junctions," *Tech. Res. Rep. Inst. Electron. Commun. Eng. Japan*, MW79-68, Sept. 1979 (in Japanese).
[19] R. Monzen, N. Ogawa, T. Anada, and J. P. Hsu, "Derivation of normal mode for dielectric planar circuit—Waveguide-type dielectric filter," *Tech. Res. Rep. Inst. Electron. Commun. Eng. Japan*, MW79-69, Sept. 1979 (in Japanese).
[20] Y. L. Chow and S. C. Wu, "A moment method with mixed basis functions for scattering by waveguide junctions," *IEEE Trans. Microwave Theory Tech.*, vol. MTT-21, pp. 333–340, May 1973.
[21] K. Matsumaru, "Reflection coefficient of *E*-plane tapered waveguides," *IRE Trans. Microwave Theory Tech.*, vol. MTT-6, pp. 143–149, Apr. 1958.

0018-9480/86/0200-0307$01.00 ©1986 IEEE